Quantum Electronics **46** (5) 437–446 (2016)

REVIEW

DOI: 10.1070/QEL15932

Passive ring resonator micro-optical gyroscopes

V.Yu. Venediktov, Yu.V. Filatov, E.V. Shalymov

Abstract. **This paper reviews recent advances in passive micro-optical gyroscopes. In the last decade, most research effort in the area of micro-optical gyros has been concentrated on a configuration that takes advantage of a single-mode passive ring resonator, which is usually fabricated using integrated optical technologies. The dimensions of such micro-optical gyros are comparable to those of micromechanical gyroscopes (area of 10 to 100 mm^2) and their sensitivity is considerably better than the sensitivity of the latter, approaching that of fibre-optic and laser gyros. Moreover, micro-optical gyros can be made as a single integrated circuit, like the micromechanical gyros, but they have no movable parts, in contrast to their micromechanical counterparts. We also describe the development and investigation of micro-optical gyros produced in our studies.**

Keywords: *passive ring resonator, interferometer, micro-optical gyroscope.*

1. Introduction

Laser and fibre-optic gyros (LGs and FOGs) form the basis of strapdown inertial navigation systems owing to a number of their advantages (broad dynamic range of velocity measurements, insensitivity to accelerations and overloads, short warm-up time and others) over traditional mechanical gyros. In spite of significant advances in this area, the LGs and FOGs cannot be used in systems for navigating compact portable movable objects because of their large size and weight. Another drawback to the optical gyros is their rather high cost. The development of relatively cheap miniature gyros (of the order of a centimetre or less in size) for a wide range of applications is a priority issue in the field of orientation and navigation devices. This niche is currently occupied by various types of micromechanical gyros, which owe their existence primarily to advances in microelectromechanical system technologies. Nevertheless, the sensitivity of the best micromechanical gyros is at least two orders of magnitude lower than that of the optical gyros. Moreover, they are sensitive to linear accelerations and various types of mechanical influences. The reason for this is that micromechanical gyro configurations include an inertia mass suspended on torsion bars. An acceleration or vibration will thus cause the movable mass to deflect from its initial position, which will be detected by a sensor as a change in angular speed. If there are considerable vibrations or accelerations (tens to hundreds of g), the angular speed cannot be measured by a micromechanical sensor [1]. The described drawbacks limit potential applications of the micromechanical gyros. The optical gyros are free from these drawbacks. In view of this, the miniaturisation of optical gyros, i.e. the ability to produce micro-optical gyros (MOGs) is currently of great practical interest.

Advances in integrated optics have laid the groundwork for research aimed at significantly reducing the cost and dimensions of optical gyros. The latter can be achieved e.g. by using a waveguide or fibre loop instead of mirror ring resonators. Lasing in a waveguide or fibre can be obtained using stimulated Brillouin scattering [2] or by doping the waveguide or fibre core with rare-earth elements [3]. The main difficulty in making active resonator MOGs is the lock-in effect, whose zone rapidly increases with decreasing perimeter. Another obstacle is the large width of the uniform gain line and a large number of associated problems, among which of special note are the complexity of obtaining stable bidirectional lasing, the multimode laser operation and instability of the amplitude of counterpropagating waves. For this reason, from the viewpoint of miniaturisation of optical gyros the most interesting possibility is a passive ring resonator (PRR) gyro.

In contrast to the resonator in the LGs, the PRR has no active element ensuring generation of counterpropagating waves. A PRR gyro was first demonstrated and investigated in the late 1970s. It had a mirror configuration and its dimensions were essentially identical to those of the LGs (a usual triangular or square configuration 20–60 cm in perimeter) [4].

In designing the first PRRs, the main purpose was to make an optical gyro similar in sensitivity to the LGs but with no lock-in zone. It was initially thought that, in the case of PRRs, locking of counterpropagating waves was impossible in principle, because there was no lasing and, accordingly, no nonlinear effects. Subsequently, the PRRs were shown to have a lock-in zone, so this PRR configuration found no wide application. A few years later, it became clear that the frequency locking in the PRRs was due to the nonlinear effects arising from the use of feedback loops. However, proper feedback loop designs allow the formation of a lock-in zone to be avoided. From the very beginning of research aimed at creating miniature optical gyros using integrated optical technolo-

V.Yu. Venediktov St. Petersburg State Electrotechnical University LETI, ul. Prof. Popova 5, 197376 St. Petersburg, Russia; Department of Physics, St. Petersburg State University, Ul'yanovskaya ul. 3, Staryi Petergof, 198504 St. Petersburg, Russia;
e-mail: vlad.venediktov@mail.ru;
Yu.V. Filatov, E.V. Shalymov St. Petersburg State Electrotechnical University LETI, ul. Prof. Popova 5, 197376 St. Petersburg, Russia;
e-mail: yvfilatov@mail.eltech.ru

Received 19 September 2015; revision received 12 February 2016
Kvantovaya Elektronika **46** (5) 437–446 (2016)
Translated by O.M. Tsarev

gies, it was clear that such a model for the PRRs is the most promising type of sensing element for MOGs [4].

2. Classification of passive MOGs according to sensing element connection

Passive MOGs can be divided into several types according to sensing element connection (Fig. 1).

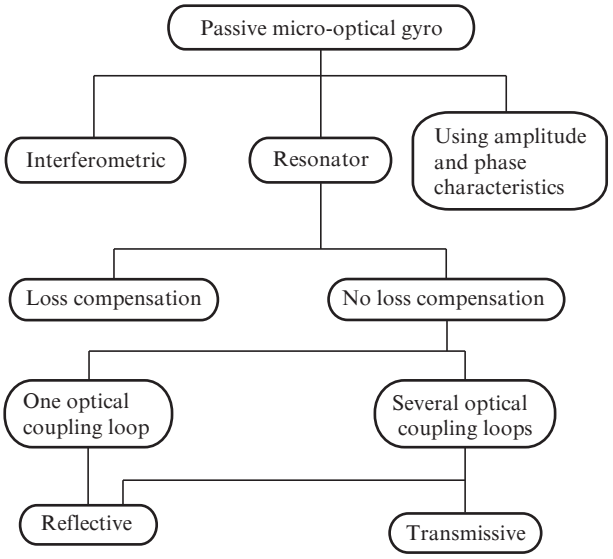

Figure 1. Types of micro-optical gyros.

2.1. Resonator MOGs

Most of the PRR MOG prototypes demonstrated to date are resonator gyros. The rotation rate of such a device is proportional to the frequency difference between the resonator eigenmodes for the two opposite propagation directions. The eigenfrequencies of the PRR can be determined from the amplitude characteristic (a dip or peak in the transmittance) of a multiple-beam ring interferometer comprising a resonator and coupler [5].

Figure 2 illustrates the working principle of the resonator MOGs. Light from a source (laser) (*1*) is divided by a beam splitter (*2*) into two waves, whose frequencies are controlled by phase modulators (*3*, *4*). Next, using a directional coupler (*9*), the light is coupled into the resonator of a ring interferometer (*10*) so that the beams from the two channels propagate in opposite directions (clockwise and counterclockwise). Through directional couplers (*7*–*9*), the light reaches photodetectors (*5*, *6*). Their signals are sent to a computer system (*11*). The optical part of the MOGs typically has the form of a uniform or hybrid integrated optical circuit (in the latter instance, optical components are fabricated on separate substrates, mounted in a package and connected by fibre). Figure 3 shows resonators used in prototype MOGs.

If a gyro is at rest with respect to inertial space, the light intensities at the inputs of the photodetectors (*5*, *6*) vary in the same way, independent of frequency. The amplitude characteristics (transmittance) of the interferometer have dips at the resonance frequencies (eigenfrequencies) f_m of the PRR, which are the same for the two opposite propagation directions in the PRR:

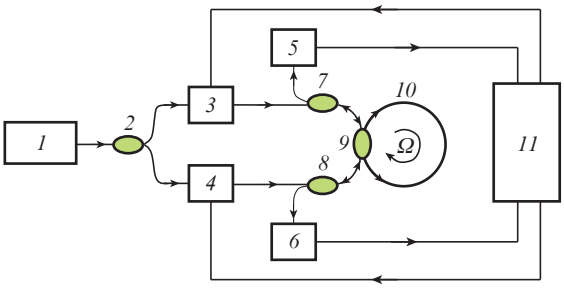

Figure 2. Working principle of the resonator MOGs.

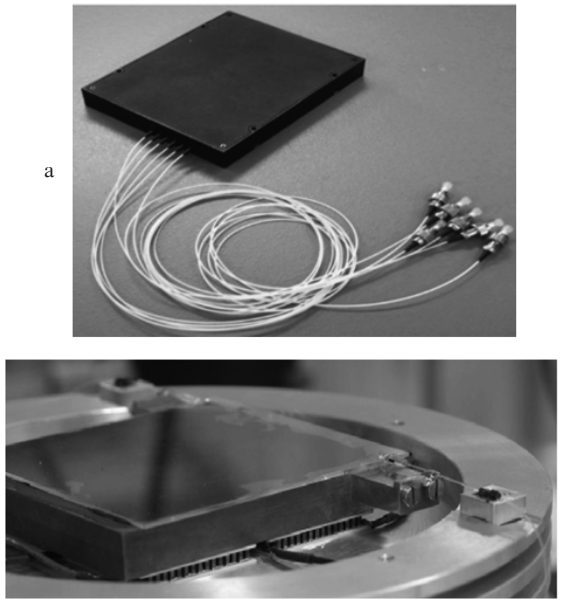

Figure 3. Appearance of the resonators of MOGs:
(a) waveguide-type PRR in a hermetically sealed package [6]; (b) PRR enclosed in a package that allows for thermal compensation and placed on a centrifuge (before tests of the MOG) [7].

$$f_m = mc/(nL), \tag{1}$$

where m is a positive integer; c is the speed of light in vacuum; n is the refractive index; and L is the resonator perimeter.

When the gyro rotates in the plane of Fig. 2, the eigenfrequencies of the PRR split because of the Sagnac effect. The difference between the eigenfrequencies for the two opposite propagation directions in the resonator is then proportional to the angular speed Ω of the MOG:

$$\Delta f = f_{m\mathrm{CCW}} - f_{m\mathrm{CW}} = \frac{4S}{\lambda_m L}\Omega, \tag{2}$$

where $f_{m\mathrm{CW}}$ and $f_{m\mathrm{CCW}}$ are the eigenfrequencies for the clockwise and counterclockwise propagation directions, respectively; S is the resonator area; $\lambda_m = c/f_m$; and $4S/(\lambda_m L)$ is the scale factor.

The computer system (*11*) determines the resonance frequencies of the PRR from the minima in the amplitude characteristic and adjusts the frequencies of the waves to them using the phase modulators. The angular speed is evaluated from the eigenfrequencies of the PRR and the scale factor. It is worth noting that the light source linewidth in a resonator

gyro should be considerably smaller than the width of the transmission minimum.

In the above resonator gyro configuration, one optical coupling loop (one additional waveguide coupled to the resonator) is used to couple light into and out of the PRR. There are also other ring resonator sensor configurations, differing in the way the signal is coupled into and out of the resonator. In almost all the resonator gyro configurations demonstrated to date, one or two bus waveguides are used to couple light into and out of the resonator. The most widespread sensor configurations are schematised in Fig. 4.

Configurations similar to that represented in Fig. 4a were considered above (Fig. 2). Configurations similar to that in Fig. 4b have the form of a ring interferometer with two optical coupling loops, one of which is used for incoupling and outcoupling light propagating in the clockwise (CW) direction, and the other, for light propagating in the counterclockwise (CCW) direction [8, 9]. Gyros that employ sensors corresponding to the configurations in Figs 4a and 4b are referred to as 'reflective'. There are also sensors in which one optical coupling loop is used to couple light into the resonator, and the other, for outcoupling the light (Fig. 4c) [10]. Gyros based on this sensor configuration are referred to as 'transmissive'.

In addition to the resonator gyros described above, there are configurations with partial loss compensation in the resonator. The higher the Q-factor of a PRR, the higher the sensitivity limit of gyros based on it [4]. The resonator Q-factor can be improved through loss compensation using a laser amplifier, while maintaining the operation of the resonator below lasing threshold. In one of the first passive resonator gyro configurations with loss compensation [11], two semiconductor optical amplifiers, A1 and A2 (Fig. 5), were placed in symmetric positions in a waveguide ring resonator. The use of semiconductor optical amplifiers allows one to compensate for the resonator loss and considerably raise the resonator Q-factor (by several orders of magnitude). One drawback to this configuration is that the waveguide resonator contains elements differing in refractive index. As a result, part of the light propagating though the semiconductor optical amplifiers is back-reflected from their facets. To avoid this, use is made of a PRR configuration with partial loss compensation, in which optical gain is ensured by active dopant atoms implanted into the resonator. Such a resonator was studied theoretically and experimentally by Hsiao and Winick [12]. The resonator was made of silicate glass doped with 2% neodymium oxide (Nd_2O_3). The structure had the form of a ring resonator with two directional couplers (Fig. 6). One bus waveguide was used for incoupling and outcoupling a test signal, and the other, for pumping the resonator. The resonator was composed of two semirings with a radius $R = 8$ mm, connected by straight line segments of length $L \sim 3$ mm. The resonator amplifier operated at a wavelength of 1.06 μm and was pumped by a semiconductor laser (150 mW, 0.83 μm). Owing to loss compensation, Hsiao and Winick [12] were able to raise the resonator Q by more than 20 times: from 8.32×10^5 (without pumping) to 1.89×10^7 (under pumping).

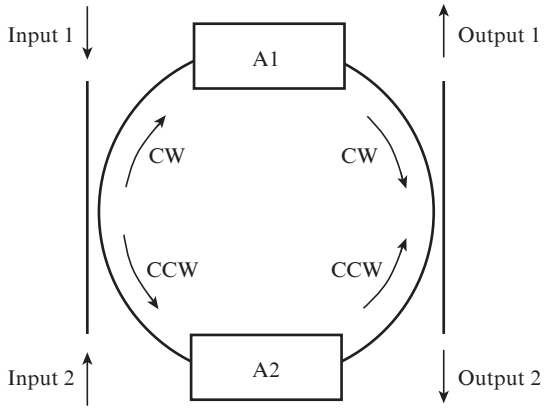

Figure 5. PRR with semiconductor optical amplifiers integrated into it [11].

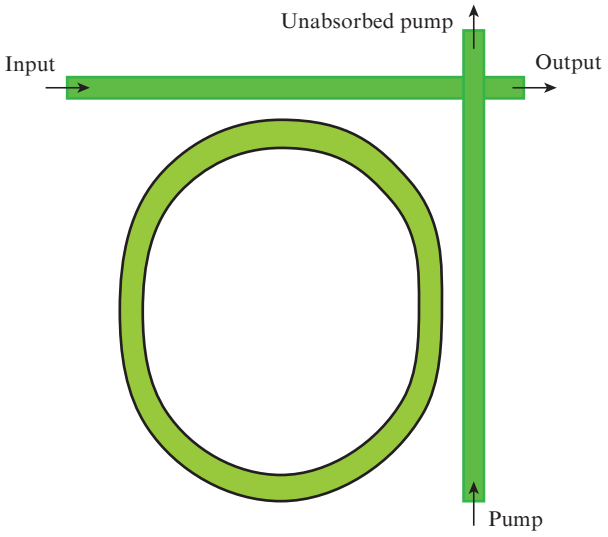

Figure 6. Resonator with a uniformly distributed loss compensation [12].

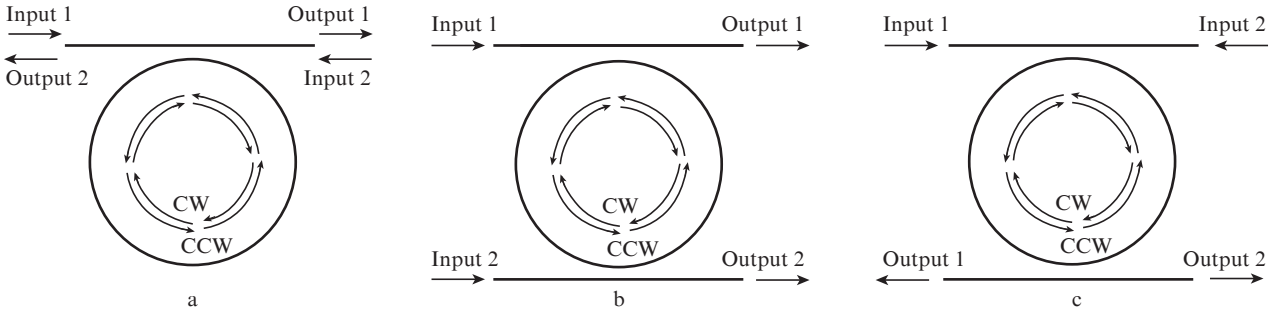

Figure 4. PRR sensor configurations.

2.2. MOGs utilising the amplitude and phase characteristics of a multiple-beam ring interferometer

As mentioned above, most of the prototype MOGs demonstrated to date are resonator gyros, which means that only the amplitude characteristic of a multiple-beam ring interferometer is used to determine the difference between the PRR eigenfrequencies, which is proportional to the angular speed. However, rotation of an interferometer leads to splitting of both its amplitude and phase characteristics. Analysis of the characteristics of a ring interferometer indicates that its phase characteristic has distinctive features near the eigenfrequencies of the resonator [13]. Since the eigenfrequency difference is proportional to the angular speed [see (2)], the phase characteristic can be used to determine it. Recently, we proposed an approach to determining the angular speed using the phase and amplitude characteristics of a multiple-beam ring interferometer [5]. The working principle and configuration of such an MOG are similar to those of resonator MOGs, but in the configuration under examination each input beam is further divided into two components, in contrast to the resonator MOGs. A PRR is used to change parameters of only one part of each input beam. Both the light passed through the PRR (test signal) and the rest of the input beam (reference signal) are directed to photodetectors. This can be achieved by replacing the directional coupler (*9*) in the configuration in Fig. 2 by a Mach–Zehnder interferometer. In this way, the reference and test information signals will be separated and joined using Y-couplers that form a waveguide Mach--Zehnder interferometer (Fig. 7). The reference and test signals will pass through different arms of the interferometer, and its sensor arm will contain the PRR.

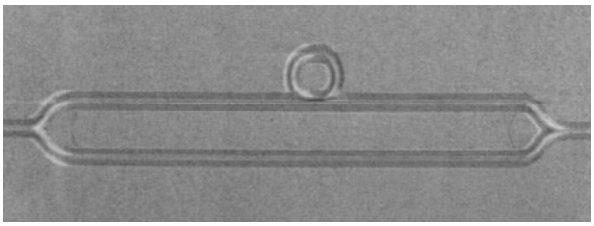

Figure 7. Waveguide Mach–Zehnder interferometer having a PRR in one of its arms [14].

When the difference between the optical lengths of the reference and sensor arms of the Mach–Zehnder interferometer is proportional to an integer number of wavelengths λ_m, the eigenfrequencies of the ring resonator correspond to minima in light intensity (in the transmittance of the optical system). From the minima in the photodetector signals, the computer system (*11*) determines the eigenfrequencies and their difference Δf, which is proportional to the angular speed. If the optical path difference is not proportional to an integer number of λ_m, the shape of the output characteristic changes (Fig. 8).

It is seen that, at any optical path difference, resonance frequencies can be determined from characteristic changes in signal intensity near the resonator eigenfrequencies. At comparatively low losses in the resonator of a ring interferometer, the use of its phase characteristic makes it possible to improve the sensitivity limit of the micro-optical gyro by an order of magnitude [15].

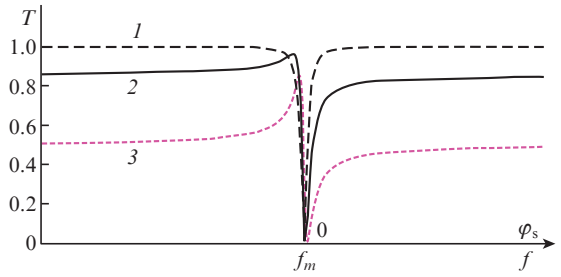

Figure 8. Relative light intensity at the photodetector input (transmittance of the optical system: $T = I/I_{in}$) when the difference between the optical lengths of the reference and sensor arms of the Mach–Zehnder interferometer is (*1*) $\lambda_m N$, (*2*) $\lambda_m(N + 1/8)$ and (*3*) $\lambda_m(N + 1/4)$, where N is an integer.

2.3. Interference MOG

The sensing element in interference MOGs is a multiturn spiral waveguide coil forming a two-beam interferometer (in contrast to the PRR MOGs, which utilise a multiple-beam interferometer). The working principle of the interference MOGs is identical to that of standard (interference) FOGs. Light is launched into the coil in two opposite directions, propagates through it and interferes at the photodetector input. The shift of the interference pattern is proportional to the rotation rate. Note that the accuracy of angular speed measurements by interference MOGs is an ambiguous function of coil length. At small interferometer dimensions (diameter of a few centimetres or less), the specific loss far exceeds that in standard FOGs because, with increasing spiral fibre length, less energy reaches the photodetector. At a certain critical spiral length, further increase leads not to higher but to lower sensitivity of the instrument. Wei et al. [16] investigated the effect of losses on the optimal spiral length (from the viewpoint of maximising accuracy). In particular, at a loss of 0.02 dB cm^{-1} the optimal resonator length was about 4.3 m.

Figure 9 shows an interference MOG configuration that utilises a rather broadband light source (with a coherence length slightly exceeding the spiral waveguide length) for minimising the effect of backscattering in the waveguide on measurement results. The input photodetector is used to monitor the input light intensity, and the other photodetector monitors the output signal. This interference gyro configuration was studied relatively recently by Srinivasan et al. [17]. They analysed a gyro with a spiral resonator 10 m in length, with a spiral spacing of 50 μm and minimum bend radius of 1 mm. The sensitivity limit of such a gyro (about 10 cm^2 in area) is

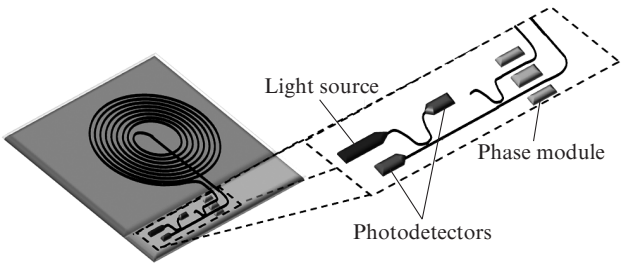

Figure 9. Interference MOG with a spiral waveguide coil [17].

19° h^{-1} at a loss of 1 dB m^{-1}. Lowering the loss to 0.1 dB m^{-1} improves the sensitivity to 4.2° h^{-1}.

There are also interferometer MOG configurations in which, instead of a waveguide spiral coil, a ring waveguide (ring resonator) [18, 19], serving as a delay line rather than as a resonator, is used. What is detected is the result of interference between two waves travelling around the closed loop in opposite directions (Fig. 10). The beam from a light source (LS) is divided by a directional coupler (DC1) into two components, which pass through modulators (M1, M2). The modulators produce a controlled phase shift between the counterpropagating waves. The light is coupled into a ring waveguide through a directional coupler (DC2) in the clockwise and counterclockwise directions. After travelling around the ring, the signals are coupled out of the waveguide and directed to a photodetector (PD), which detects two-beam interference. The waveguide here acts as a multiturn coil whose equivalent number of turns, N, corresponds to the number of round trips in the PRR. The number of round trips is determined by the loss in the waveguide and its perimeter. To prevent the light beams arriving after different numbers of round trips from overlapping (to avoid multiple-beam interference), use is made of pulsed phase modulation with a pulse width equal to the loop round trip time and a repetition frequency period greater by $N + 1$ times [18].

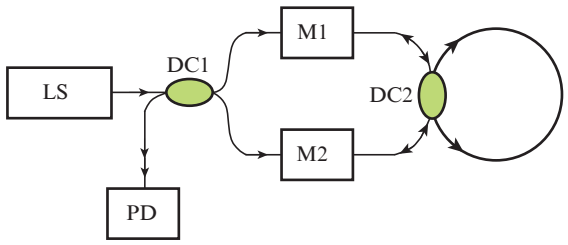

Figure 10. Ring waveguide interference MOG [18].

The MOG schematised in Fig. 10 is a reflective gyro. Also possible are transmissive MOGs. Interference MOG configurations that utilise a closed-loop waveguide instead of a spiral waveguide coil are sometimes referred to as interference–resonator or re-entrant MOGs.

3. Classification of the passive MOGs according to the sensing element design

The key component of the micro-optical gyros is their PRR. It is the PRR that determines the fabrication process of the entire instrument and the sensitivity limit, minimal dimensions and many other characteristics of the gyro. The passive MOGs can be classified according to the design of their sensing element (Fig. 11).

3.1. Planar resonators

Most experimental setups and passive MOG prototypes are designed and fabricated from elements produced using planar (integrated) optics. The reason for this is that the use of integrated optical technologies makes it possible to reduce the weight, dimensions, energy consumption and cost of instruments and facilitates temperature control. Moreover, planar

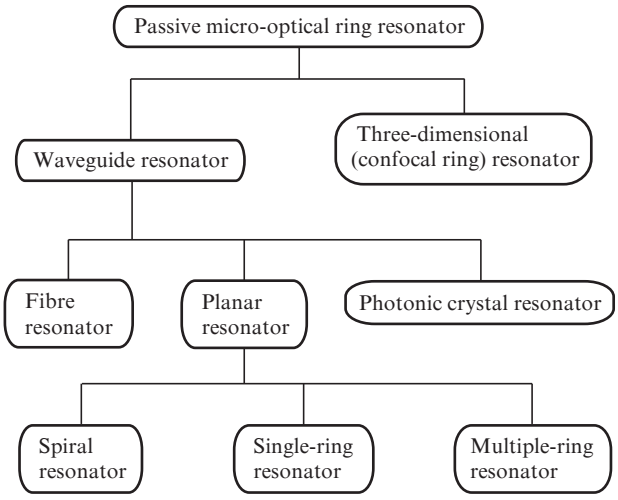

Figure 11. Classification of the MOGs according to the design of their sensing elements.

gyros can be made as a single integrated optical configuration, which improves the reliability of the instrument.

3.1.1. Single-ring resonators. High-Q resonators ($Q > 10^5$) formed by one closed-loop single-mode waveguide a few centimetres or less in diameter (single-ring resonators) are most often used as sensing elements in passive MOGs. The sensitivity of a gyro is then essentially determined by the Q-factor of the resonator (resonator loss) and its area [4]. At present, a variety of materials are used to fabricate high-Q waveguide ring resonators: silica on silicon (SOS), silicon nitride (Si_3N_4), lithium niobate ($LiNbO_3$), glass, indium phosphide (InP), polymers and others.

Very low losses in a ring resonator can be achieved e.g. using SOS technology. SOS waveguides are commonly produced by chemical vapour deposition, flame hydrolysis deposition or rf plasma chemical vapour deposition in combination with ion etching techniques. SOS technology enabled the fabrication of resonators with losses under 0.01 dB cm^{-1} and Q-factor above 10^7 [20]. Later, the potentialities of SOS structures were demonstrated by Guo et al. [21]. The sensitivity limit of an SOS resonator gyro was shown to be 1.6° h^{-1}.

There are also other technologies that allow for the fabrication of low-loss bent waveguides. For example, resonators suitable for MOGs can be produced through ion exchange in glass or titanium diffusion in $LiNbO_3$. From the viewpoint of loss minimisation, these materials are somewhat inferior to SOS, but the fabrication of glass waveguides through ion exchange is a simpler and cheaper process, which enables waveguides to be doped with particular impurities (for example Nd_2O_3) necessary for loss compensation [12]. Similar advantages are offered by $LiNbO_3$ waveguides [22].

Relatively recently, several reports described high-Q Si_3N_4 resonators on silicon substrates (see e.g. Refs [23, 24]). Tien et al [23] assessed the quality factor of Si_3N_4 ring resonators at several wavelengths. With a ring waveguide of 5.3 μm width, 50 nm thickness and 5 mm radius, the quality factor of the resonator was 1×10^6, 28×10^6 and 19×10^6 at wavelengths of 1550, 1310 and 1060 nm, respectively. Later, Spencer et al. [24] studied a resonator formed by a ring waveguide of 7 μm width, 45 nm thickness and 9.8 mm radius. Its quality factor was 3.5×10^7.

Yet another material that can be utilised in the fabrication of sensing elements for MOGs is InP. Ciminelli et al. [25] were the first to demonstrate a ring resonator with a quality factor of $\sim 10^6$ in the form of an InGaAsP ring waveguide of 2 μm width, 0.3 μm thickness and 13 mm radius on an InP substrate. The resonator was produced using metal-organic vapour phase epitaxy, photolithography and reactive ion etching. The sensitivity limit of a gyro based on this resonator was estimated at $10° \text{ h}^{-1}$ [25].

Other materials, e.g. some polymers, can also be used in the fabrication of passive ring resonators. The use of polymer materials allows one to reduce the production cost of integrated optical instruments. Unfortunately, most polymers are unsuitable for the fabrication of sensing elements for MOGs because of the high transmission loss. Qian et al. [26] considered a polymer-based resonator with a quality factor of $\sim 10^5$. The width, thickness and radius of curvature of the ring waveguide were 0.5 μm, 0.5 μm and 5 mm, respectively. The sensitivity limit of MOGs based on state-of-the-art polymer PRRs is no better than tens of degrees per hour.

3.1.2. Multiple-ring resonators. Recent years have seen increasing interest in micro-optical multiple-ring resonators as sensing elements of MOGs [27–38]. Note that two basic structures are distinguished. One of them (Fig. 12a) has the form of a chain of optically coupled resonators (chain resonator in what follows), and the other (Fig. 12b) consists of several ring resonators optically coupled to one bus waveguide (bead resonator in what follows).

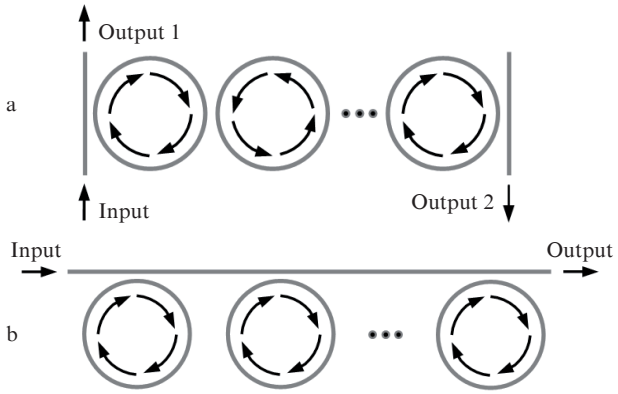

Figure 12. (a) Chain and (b) bead resonators.

As a rule, chain resonators consist of an array of high-Q miniature PRRs (from a few to tens of microns in diameter). Neighbouring resonators in the array are tunnelling-coupled to each other to form a coupled resonator optical waveguide (CROW). At present, there is no generally accepted opinion as to the sensitivity of gyros based on such structures. Terrel et al. [27, 28] think that it does not exceed the sensitivity of MOGs based on single-ring resonators with the same area as chain resonators. At the same time, in a number of reports [29–31] the opposite is stated explicitly or implicitly. Comparison of the sensitivity of MOGs based on such resonators is complicated by the great diversity of chain structures [32, 33].

There are a variety of chain resonator gyro configurations. The simplest configuration, shown in Fig. 12a, has often been the subject of analysis [29, 30, 34]. A great deal of attention has also been paid to a structure consisting of a bent chain of identical PRRs (Fig. 14) with identical coupling coefficients. Bus waveguides optically coupled to the end resonators are terminated with directional couplers. An input signal is divided by a coupler into two waves which travel around the resonator in opposite directions. Returning to the coupler, the counterpropagating waves interfere and travel to the output of the structure [31]. The sensor uses an interferometric scheme for connecting the sensing element. The sensitivity limit of a gyro based on such a structure consisting of nine rings of 25 μm radius is about $1° \text{ h}^{-1}$. Note that, to reach this value, the Q-factor of each ring resonator should be 10^7. However, a Q-factor of 10^4 to 10^5, typical of micro-optical waveguide ring resonators of 25 μm radius, significantly degrades the sensitivity of the sensor [35].

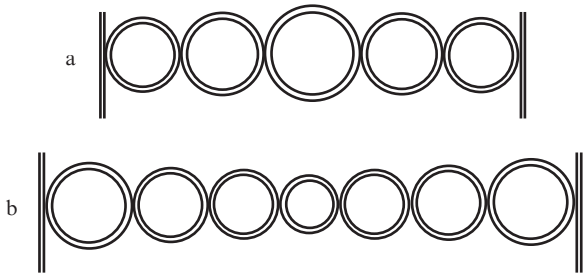

Figure 13. Chain resonator made up of PRRs differing by an integer number of wavelengths, with the resonator perimeter uniformly (a) decreasing and (b) increasing from the centre to the periphery [32].

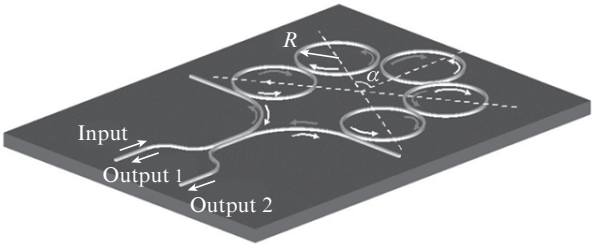

Figure 14. Chain resonator sensor [31].

In the configuration considered by Sorrentino et al. [33], identical optically coupled ring resonators are aligned in a straight line. The coupling coefficients between the waveguides differ (take two values) and alternate starting in the centre, as shown in Fig. 15 (the dark and light rectangles represent stronger and weaker optical coupling, respectively). This coupling coefficient distribution allows the sensitivity of the device to rotation to be improved by several orders of magnitude, in contrast to a uniform distribution. As pointed out by Sorrentino et al. [33], with this configuration a MOG

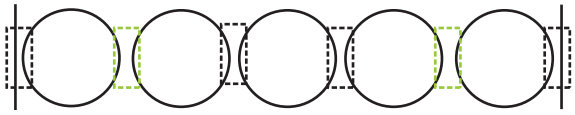

Figure 15. Chain resonator with alternating coupling coefficients [33].

sensitivity limit of 0.002° h^{-1} can be achieved (CROW made up of 21 rings with a radius of 50 μm).

There is also interest in chain resonator configurations made up of PRRs of different sizes [32, 36]. Toland et al. [32] compared structures consisting of identical resonators (Fig 12a) and similar arrays made up of resonators of different sizes (Fig. 13). The configurations considered by them comprise an odd number of PRRs symmetric with respect to the centre of the structure. The perimeters of any two neighbouring resonators differ by an integer number of wavelengths. Such configurations allow the sensitivity to rotation to be improved relative to a standard configuration (Fig. 12a). In particular, the sensitivity of a device consisting of five coupled resonators with perimeters differing by λ corresponds to that of a standard gyro structure made up of 35 resonators [32].

Nevertheless, despite the promising results of theoretical calculations, there are a number of problems related to practical implementation of chain resonator gyros. The point is that the fabrication of such structures cannot be free of random variations in the size of the ring resonators and coupling between them. The sensitivity of the chain gyros is not influenced by variations in coupling coefficients, but even slight changes in the size of the ring resonators significantly degrade it [30].

Another type of multiple ring (bead) resonator is less sensitive to variations in the size of the component PRRs: variations within 0.1 μm have essentially no effect on the sensitivity of the structure [37]. Consider several configurations of such resonators. A bead structure considered theoretically by Matsko et al. [38] consisted of a bus waveguide bent in the form of a ring and a large number of high-Q micro-optical resonators located on the two sides of the bus waveguide (Fig. 16a), whose ends were used to couple the signal in and out. 'Whispering gallery' resonators were proposed by Matsko et al. as high-Q micro-optical resonators constituting the structure.

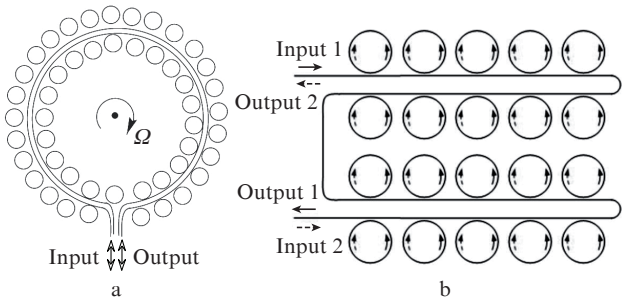

Figure 16. Bead structures in which PRRs are located (a) on both sides [38] and (b) on one side [37] of a bus waveguide.

Yet another configuration of a compact bead structure for angular speed sensing was reported by Tian et al. [37]. In contrast to that above, all the ring resonators in this configuration are coupled to only one side of a bus waveguide (Fig. 16b). Unfortunately, no data were reported on the sensitivity limit of gyros based on the above structures [37, 38].

Even the most promising multiple ring resonator configurations have not yet been realised in practice. Recent theoretical studies [27–36] showed however that the accuracy limit of gyros based on such resonators can be several orders of magnitude higher than that of micromechanical systems of comparable dimensions.

3.1.3. Spiral resonators. Yet another promising type of sensing element in MOGs is a spiral waveguide resonator. The idea to use a spiral waveguide coil for producing a cheap and compact gyro emerged rather long ago [4], but this type of resonator was not intensely studied until recently. The reason for this is that the ability to fabricate a high-Q miniature spiral waveguide coil is a technological challenge, which can only be overcome using cutting-edge integrated optical technologies.

Consider two spiral resonator configurations [17, 39]. One of them (Fig. 9) is a two-beam resonator. The ends of the spiral fibre form a directional coupler. The coupling coefficient between them should be near 50%, which ensures the highest sensitivity of the gyro to rotation. The sensitivity limit of the waveguide spiral resonator gyro was reported to be 19° h^{-1} [17]. Attention was also paid to a resonator consisting of several layers of series connected spiral waveguides stacked on top of each other and connected using vertical directional couplers. Such a design makes it possible to reduce the area occupied by the sensor. At the same time, it increases the loss in the resonator through the loss arising from light transitions between neighbouring layers (0.02 dB per transition), which degrades the sensitivity of the device [17]. With future advances in integrated optical technologies, the optical loss per transition between layers is expected to be considerably reduced and the use of multilayer architectures may become justified.

Another type of spiral waveguide resonator (Fig. 17) is a multiple-beam ring resonator [39]. Research was focused on a scheme consisting of a PRR in the form of a closed-loop spiral waveguide and two bus waveguides coupled to the main waveguide through directional couplers. Use was made of single-mode (6 × 6 μm) germanium-doped silicon (n = 1.457) waveguides. The spiral fibre length was 42 cm and the area occupied by it on a substrate was 20 cm^2. The propagation loss in a closed-loop waveguide was 0.1 dB cm^{-1} and the additional loss due to spiral intersection was under 0.01 dB. The experimentally determined Q-factor of the described resonator exceeded 1.5×10^6, which corresponds to a sensitivity of 156° h^{-1} in a gyro based on it. As pointed out by Ciminelli et al. [39], the sensitivity of such a sensor can be improved to 10° h^{-1} by reducing the propagation loss in the spiral fibre to 0.05 dB cm^{-1} (which is achievable at present) and the input/output loss to 1–2 dB (typical value).

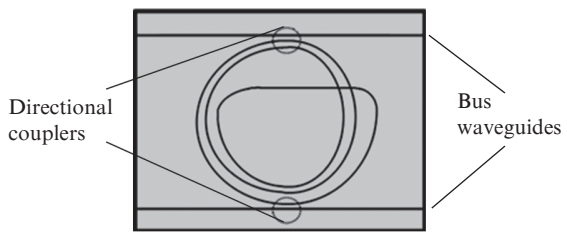

Figure 17. Spiral PRR sensor [39].

3.2. Photonic crystal resonator

Photonic crystals are materials with an ordered structure characterised by a strictly periodic variation in the refractive index on a length scale comparable to wavelengths in the vis-

ible and near-IR spectral regions. Any inhomogeneity in a photonic crystal is thought to be a defect. An electromagnetic field is concentrated in such regions, which is used in photonic crystal microresonators and waveguides [40].

A high-Q photonic crystal PRR can be fabricated from a variety of one-dimensional (1D) photonic crystals. Ciminelli et al. [41] considered an SOS PRR in the form of a ring Bragg grating (Fig. 18a). Calculations indicate that the state of the art in integrated optics allows for the fabrication of such resonators about 5 cm in diameter with a Q-factor above 10^9. Another type of 1D photonic crystal that can be used for the fabrication of PRRs is a closed planar semiconductor waveguide with a 1D periodic hole array (Fig. 18b) [42].

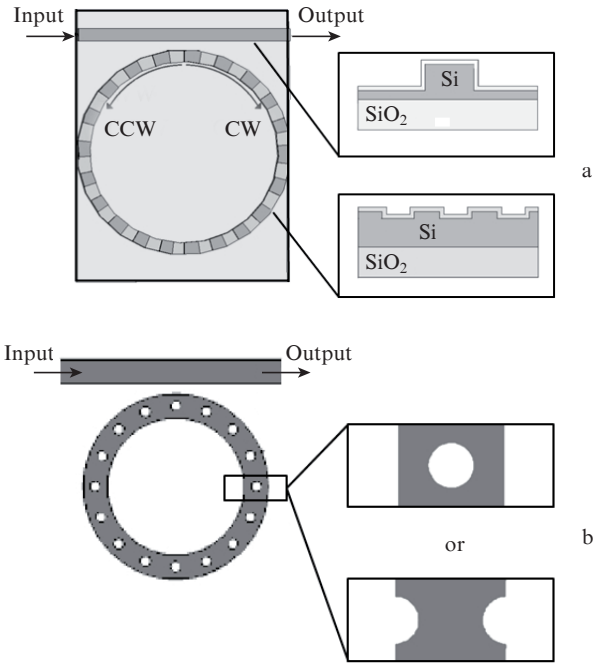

Figure 18. One-dimensional photonic crystal PRRs in the form of a (a) closed Bragg grating [44] and (b) closed perforated waveguide [43].

Considerable potential for the fabrication of high-Q ($Q > 10^6$) micro-optical PRRs is offered by a photonic crystal structure in the form of a planar semiconductor waveguide with a periodic 2D hole array. It is also easy to produce a photonic crystal PRR by creating a defect in the form of a hexagon (Fig. 19), whose thickness and size will determine the eigenmode composition and finesse of the resonator [45].

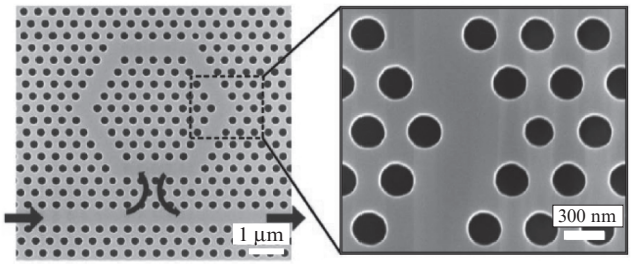

Figure 19. Photonic crystal PRR [45].

As shown in an analytical study of the Sagnac effect in photonic crystal resonators [46], its rotation leads to splitting of the resonance frequencies of counterpropagating waves. Assessment of the effect in particular photonic crystals indicates that the scale factor in them (1.6×10^{-2} rad s^{-1}) is much less than that in passive MOGs (calculations were performed for a photonic crystal PRR about 0.93 μm in radius, with a Q-factor of 10^4). As pointed out by Steinberg and Boag [46], the sensitivity of such resonators is still insufficient for practical implementation of MOGs. However, photonic crystal PRRs have been demonstrated that have a much higher Q ($Q > 10^6$) [41, 45], and the size of such resonators can also be increased. In this context, photonic crystal PRRs are potentially attractive sensing elements for MOGs.

3.3. Loop resonator

A classic fibre resonator (multiturn fibre coil) is unsuitable as a sensing element of MOGs because of the sharp increase in loss as the coil diameter decreases to a few centimetres or less. However, Sumetsky et al. [47] have recently proposed, fabricated and investigated a compact high-Q fibre PRR which is a miniature version of a fibre resonator proposed as early as 1982 [48] and consisting of a single turn of single-mode fibre whose ends are connected to a directional coupler (Fig. 20a). A distinctive feature of the miniature version is that the resonator region where portions of the fibre superpose acts as a directional coupler (Fig. 20b).

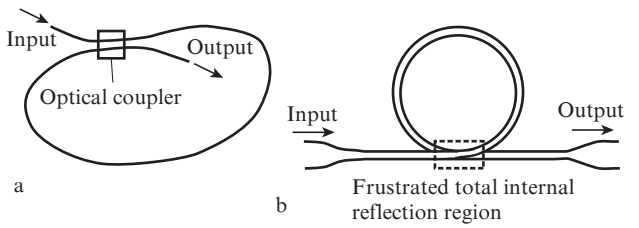

Figure 20. (a) Macroscopic [48] and (b) microscopic [47] versions of a loop PRR.

To date, micro-optical fibre resonators about 0.5 mm in radius with a Q-factor above 6×10^6 at a fibre diameter of ~1 μm have been demonstrated (Fig. 21). The fabrication of such resonators involves microfibre drawing and bending into an optically coupled loop. The microfibre to be drawn is placed in a sapphire capillary tube, which is then heated by

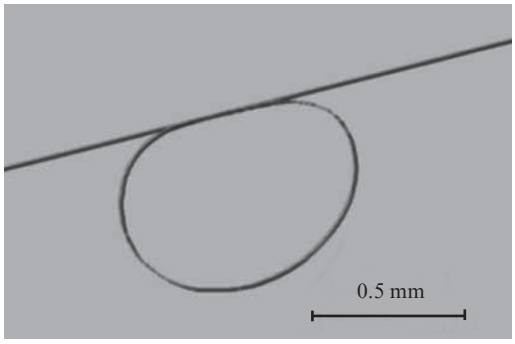

Figure 21. Micro-optical fibre resonator [47].

the beam of a commercially available laser (e.g. a CO_2 laser). In such a microscopic furnace, the fibre is drawn until its diameter reaches the desired level (~1 μm or less) (Fig. 22a). Next, the fibre is twisted into an optically coupled loop using several manipulators (Fig. 22b). Surface (electrostatic or van der Waals) forces help to join the ends of the loop.

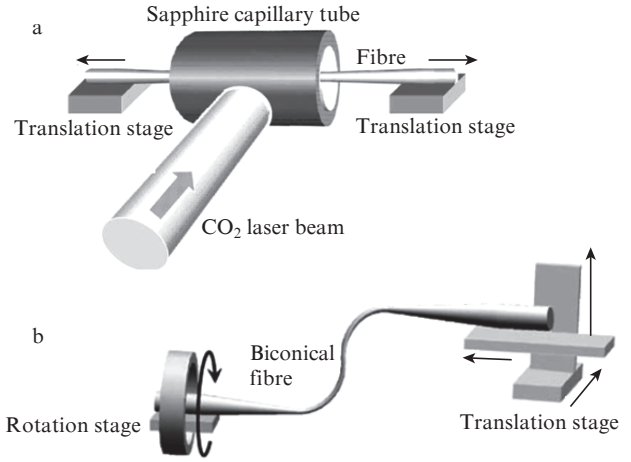

Figure 22. Fabrication of micro-optical fibre resonators [47] by (a) fibre drawing and (b) micro-optical loop resonator twisting.

To protect such a resonator from mechanical influences, it can be coated with a low refractive index polymer [49]. The advantages of the micro-optical fibre loop resonators over waveguide resonators are that they are easy to fabricate and have a low production cost.

3.4. Confocal ring resonator

In most reports concerned with MOGs, planar single-mode waveguide resonators are predominantly considered to be suitable sensing elements. As in all passive optical gyro systems, multimode waveguides cannot be used in this case because of the modal dispersion. For the same reason, most 3D resonators also cannot be used. Nevertheless, one can realise a confocal ring resonator – a 3D PRR whose focal points are brought into coincidence and whose spectrum is characterised by degeneracy of the frequencies of its higher transverse modes (a set of equidistant modes) [50]. A resonator possessing such properties can serve as a sensing element of a MOG.

In the paraxial approximation, one can obtain a confocal ring resonator using flat and concave torus-like reflective surfaces [51]. However, the paraxial approximation cannot be used in calculations for a micro-optical resonator. In a non-paraxial approach, a confocal ring resonator can be obtained using flat and concave parabolic astigmatic reflective surfaces [51]. One possible configuration is shown in Fig. 23. The reflective surfaces *1*, *3* and *4* are flat and surfaces *2* are parabolic astigmatic reflective surfaces with different principal focal lengths: $F_1 = 2a/\cos\vartheta$ in the plane of incidence and $F_2 = 2a\cos\vartheta$ in an orthogonal plane.

Thus, a 3D passive ring resonator can be used as a sensing element of a micro-optical gyro instead of a planar single-mode ring resonator. Confocal resonators have a number of advantages over planar ones. At small resonator dimensions (diameter of several centimetres or less), a planar ring resonator has higher losses because the large curvature of the ring waveguide leads to frustrated total internal reflection. The losses in a confocal ring resonator do not increase with decreasing resonator size. At a resonator diameter of several centimetres, the resonator loss is one to four orders of magnitude lower (depending on the quality of the reflective surfaces). One drawback to confocal ring resonators is that a relatively complex process is needed for producing their parabolic astigmatic reflective surface. Such a resonator can be fabricated e.g. by diamond machining.

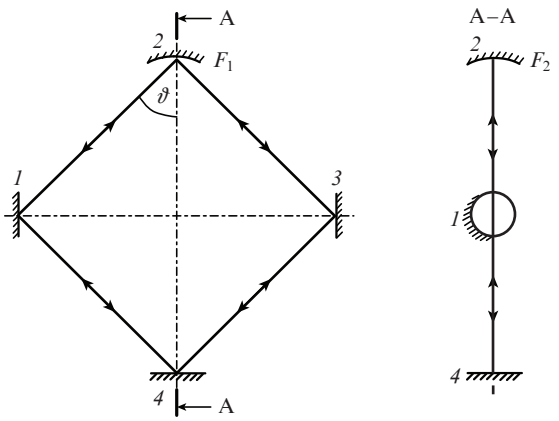

Figure 23. Confocal ring resonator.

4. Conclusions

This paper has reviewed recent advances in passive MOGs. In the last decade, most research effort has been concentrated on a configuration that uses a single-mode passive ring resonator, which is usually fabricated using integrated optical technologies. We have also considered other technologies that enable the fabrication of passive resonators suitable for MOGs. Several micro-optical gyro prototypes have been produced and investigated to date. Analysis of recent advances in MOG configurations allows us to hope that micro-optical sensors with sensitivity of the order of $10^\circ\ h^{-1}$ or better will enter the marketplace in the coming decade.

Acknowledgements. This work was supported by the Russian Science Foundation (RSF Grant No. 14-19-00693). V.Yu.V. acknowledges the support of the RF Ministry of Education and Science (Scientific Research Organisation and Implementation State Task, basic stage).

References

1. Ciminelli C., Dell'Olio F., Campanella C.E., Armenise M.N. *Adv. Opt. Photonics*, **2** (3), 370 (2010).
2. Culshaw B. *Meas. Sci. Technol.*, **17** (1), R1 (2006).
3. Liu K., Zhang W., et al. *J. Micromech. Microeng.*, **19**, 113001 (2009).
4. Boronakhin A.M., Luk'yanov D.P., Filatov Yu.F. *Opticheskie i mikromekhanicheskie inertsial'nye pribory* (Optical and Micromechanical Inertial Devices) (St. Petersburg: Elmor, 2008).
5. Venediktov V.Yu., Filatov Yu.V., Shalymov E.V. *Kvantovaya Elektron.*, **44** (12), 1145 (2014) [*Quantum Electron.*, **44** (12), 1145 (2014)].
6. Liang N., Lijun G., et al. *J. Semicond.*, **35** (12), 124008 (2014).
7. Vannahme C., Suche H., Reza S., Ricken R., Quiring V., Sohler W. *Proc. Europ. Conf. Integrated Optics* (WE1, 2007).
8. Chevalier J.R. European Patent, EP 0744594 (1996).

9. Strandjord L.K., Salit M.K. European Patent, EP 2813815 (2014).
10. Feng L., Wang J., Zhi Y., et al. *Opt. Express*, **22** (22), 27565 (2014).
11. Ciminelli C., Peluso F., Armenise M.N. *Proc. SPIE Int. Soc. Opt. Eng.*, **5728**, 93 (2005).
12. Hsiao H.K., Winick K.A. *Opt. Express*, **15** (26), 17783 (2007).
13. Filatov Y.V., Shalymov E.V., Venediktov V.Y. *Proc. SPIE Int. Soc. Opt. Eng.*, **9141**, 91411B (2014).
14. Absil P.P., Hryniewicz J.V., Little B.E., Wilson R.A., Joneckis L.G., Ho P.-T. *IEEE Photonics Technol. Lett.*, **12** (4), 398 (2000).
15. Venediktov V.Y., Filatov Y.V., Shalymov E.V. *Proc. SPIE Int. Soc. Opt. Eng.*, **9506**, 95061N (2015).
16. Wei W., Junlei X., Yuxin X. *Proc. IEEE*, **10478339**, 1 (2008).
17. Srinivasan S., Moreira R., et al. *Opt. Express*, **22** (21), 24988 (2014).
18. Zhang Y.S., Ding H.G. *Vestnik MGTU im. N.E.Baumana. Ser. Priborostroenye*, **2005** (4), 109 (2005).
19. Carroll R. United States Patent, US 5420684 (1995).
20. Adar R., Serbin M.R., Mizrahi V. *J. Lightwave Technol.*, **12** (8), 1369 (1994).
21. Guo L., Shi B., Chen C., Zhao M. *Optik*, **123** (4), 302 (2012).
22. Das B., Ricken R., Quiring V., et al. *Opt. Lett.*, **29** (2), 165 (2004).
23. Tien M.C., Bauters J.F., Heck M.J.R., Spencer D.T., Blumenthal D.J., Bowers J.E. *Opt. Express*, **19** (14), 13551 (2011).
24. Spencer D.T., Tang Y., Bauters J.F., Heck M.J.R., Bowers J.E. *Proc. IEEE*, **13149871**, 141 (2012).
25. Ciminelli C., Dell'Olio F., Armenise M.N., Soares F.M., Passenberg W. *Opt. Express*, **21** (1), 556 (2013).
26. Qian G., Tang J., Zhang X.Y., Li R.Z., Lu Y., Zhang T. *J. Nanomater.*, **2014**, 146510 (2014).
27. Terrel M.A., Digonnet M.J.F., Fan S. *J. Lightwave Technol.*, **27** (1), 47 (2009).
28. Terrel M.A., Digonnet M.J.F., Fan S. *Laser Photonics Rev.*, **3** (5), 452 (2009).
29. Kalantarov D., Search C.P. *Opt. Lett.*, **39** (4), 985 (2014).
30. Florio F., Kalantarov D., Search C.P. *J. Lightwave Technol.*, **32** (21), 4020 (2014).
31. Scheuer J., Yariv A. *Phys. Rev. Lett.*, **96** (5), 053901 (2006).
32. Toland J.R.E., Kaston Z.A., et al. *Opt. Lett.*, **36** (7), 1221 (2011).
33. Sorrentino C., Toland J.R.E., Search C.P. *Opt. Express*, **20** (1), 354 (2012).
34. Peng C., Li Z., Xu A. *Opt. Express*, **15** (7), 3864 (2007).
35. Armenise M.N., Ciminelli C., Dell'Olio F., Passaro V.M.N. *Advances in Gyroscope Technologies* (Heidelberg: Springer, 2010).
36. Zhang Y., Wang N., et al. *Phys. Lett. A*, **372** (36), 5848 (2008).
37. Tian H., Zhang Y., Zhang X., Wu H., Yuan P. *Opt. Express*, **19** (10), 9185 (2011).
38. Matsko A.B., Savchenkov A.A., Ilchenko V.S., Maleki L. *Opt. Commun.*, **233** (1), 107 (2004).
39. Ciminelli C., Dell'Olio F., Armenise M.N. *IEEE Photonics J.*, **4** (5), 1844 (2012).
40. Akahane Y., Asano T., Song B.S., Noda S. *Nature*, **425** (6961), 944 (2003).
41. Ciminelli C., Campanella E.C., Armenise M.N. Europ. Patent, EP 2917691 (2013).
42. Goldring D., Levy U., Mendlovic D. *Opt. Express*, **15** (6), 3156 (2007).
43. Zhang Y., Zeng C., Li D., Gao G., et al. *Opt. Lett.*, **39** (5), 27 (2014).
44. De Leonardis F., Campanella C.E., et al. *Sensors*, **14**, 16017 (2014).
45. Zhang Y., Zeng C., Li D., Gao G., et al. *Opt. Lett.*, **39** (5), 1282 (2014).
46. Steinberg B.Z., Boag A. *J. Opt. Soc. Am. B*, **24** (1), 142 (2007).
47. Sumetsky M., Dulashko Y., Fini J.M., Hale A., DiGiovanni D.J. *J. Lightwave Technol.*, **24** (1), 242 (2006).
48. Stokes L.F., Chodorow M., Shaw H.J. *Opt. Lett.*, **7** (6), 230 (1982).
49. Xu F., Pruneri V., Finazzi V., Brambilla G. *Opt. Express*, **16** (2), 1062 (2008).
50. Shalymov E.V. *Izv. SPbGETU LETI*, **4**, 64 (2015).
51. Filatov Y.V., Sevryugin A.A., et al. *Opt. Eng.*, **54** (4), 044107 (2015).